*16th World Conference on Earthquake, 16WCEE 2017*

*Santiago Chile, January 9th to 13th 2017*

*Paper N° 3778*

*Registration Code: S-X1461230614*

# A PRELIMINARY INVESTIGATION OF METHODS FOR ESTIMATING THE PROBABILITY OF FAILURE FOR ROCKING BODIES.

M. Garcia Espinosa[(1)], M.N. Chatzis[(2)]

*[(1)] PhD Candidate in Dept. of Engineering Science, University of Oxford, United Kingdom, maria.garciaespinosa@eng.ox.ac.uk*
*[(2)] Associate Professor in Dept. of Engineering Science, University of Oxford, United Kingdom, manolis.chatzis@eng.ox.ac.uk*

## *Abstract*

For reasons related to functionality, mobility, or as recently has been suggested to improve dynamic performance, several structural and non-structural elements are let to experience large rotations and displacements when subjected to ground excitations. This overall behavior can be characterized as rocking. Recently, the interest in the behavior of rocking elements subjected to ground motions has increased. This is partly due to the importance of the rocking bodies themselves, for example museum artifacts and monuments are irreplaceable, while hospital equipment is of paramount importance to post-seismic response, partly due to the fact that advances in technology have allowed for key elements of infrastructure to become more mobile, such as large super-computer units, and finally also due to the realization that a large part of the cost during earthquakes is attributed to non-structural elements. Characterizing the risk of these elements subjected to ground motions is therefore of increasing importance.

However, the dynamic response of rocking elements during ground motions is strongly non-linear and the mode of failure of these objects is, unlike typical civil engineering applications, not related to exceeding a stress- but a displacement -or rotations - limit. Consequently, several of the existing methodologies to study the risk associated of structures are not applicable, as they usually are focused on systems that are geometrically linear and whose failure is associated with fracture or yield. A remedy for this is to study the risk associated to rocking bodies using the more general approach of creating probability of failure curves. The latter approach requires the use of time histories compatible with some measure of intensity as an input to the deterministic models. For this purpose there are several alternatives: stochastic methods able to generate synthetic time histories, such as the Spectral Representation method, methods based on selecting or scaling existing recorded ground motions based on their compatibility to an intensity measure, and numerical data driven approaches able to generate new time histories based on a set of selected time histories. Each of the previous methods has properties which may be more or less advantageous when applied to the problem of rocking. This work will focus on generating ground records compatible with a seismological intensity measure, the magnitude of the earthquake, for the purpose of generating probability of failure curves for rocking bodies. The effects of biaxial versus uniaxial input will be examined highlighting the importance of making use of the notion of principal axes. Based on this conclusions a methodology for creating probability of failure curves for rocking bodies will be proposed.

*Keywords: Rocking, primary axes, earthquake generation, stochastic model*

# 1. Introduction

The stability of free-standing bodies subjected to ground motions is a problem of significant importance, as for example illustrated in the Loma Prieta earthquake in 1989 where many art objects were damaged [1]. These objects differ to standard structural systems in that their primary mode of failure is mainly associated to displacement- rather than stress- based criteria of failure, and that their response is mainly associated to rigid body rather than deformation modes. Hence, there is a need of suitable deterministic and stochastic models that allow for estimating the ground motion related risk of such objects.

The most popular model for the response of free standing rocking bodies, the Inverted Pendulum Model (*IPM*) was suggested by Housner in [2].The model makes the assumptions of planar response, no sliding, no free-flight mode and that both the body and the support medium are rigid. While a series of following papers have illustrated the significance of these neglected phenomena [3, 4, 5, 6, 7, 8], its study allows for valuable qualitative conclusions.

Studies of the response of rocking bodies subjected to cycloidal pulses [2, 9, 10] have shown a series of interesting properties of the system. However, ground motions cannot in general be perfectly approximated with idealized pulses. Estimating the risk of rocking bodies subjected to ground motions requires the generation or selection of a reasonable number of earthquakes so as to accurately estimate the probability of failure and create fragility curves by varying the intensity measure. Hence, one of the key challenges in this problem is how these ground motions are produced. The methods that have been proposed in the literature for the purpose can be classified into three broad categories: selecting and potentially scaling recorded ground motions as in [11], generating artificial ground motions based on underlying stochastic [12, 13] or seismological models[14, 15], and generating new records from a list of selected recorded motions[16, 17, 18].

In terms of estimating the risk of rocking bodies subjected to ground motions, generated artificial records using the spectral representation method [12] and the Kanai-Tajimi-Clough-Penzien spectrum [19] are used in [20]. In [14] the peak ground acceleration is used, a source point model was used in [21], and selected recorded motions were used in [22].

In this work the ground motion generation model suggested in [17] and [18] is used. In [17] the simulation of artificial time-histories is achieved through a fully Non-Stationary (NS) stochastic model. This approach uses a list of selected recorded earthquakes from the NGA database [23] to calibrate the parameters of the model in terms of seismic characteristics. The work in [18] extends the model for the generation of biaxial inputs in terms of the principal components. The goal of the current work is to generate the probability of failure curves for a rocking body using the *IPM*, paired with uniaxial and biaxial inputs generated according to [17, 18] respectively using the magnitude of the earthquake as an intensity measure. A discussion follows on the effects of the direction of the input on the stability of the body together with the benefits of using biaxial inputs even for problems of planar rocking.

# 2. Inverted Pendulum model

This section provides a brief description of the *IPM*, developed by Housner in [2] which is the model used in this paper. The rocking body, the properties and the axes convention used in the following equations are defined in Fig. 1 . The rigid body is defined by its mass, *m*, and its moment of inertia, $I_0$, about either corners $0$ and $0'$.The half-width and half-height of the body are defined by *b* and *h*, respectively. $R = \sqrt{h^2 + b^2}$ is the distance from a corner to the center of mass and the angle $\alpha = \tan^{-1} b/h$ describes the slenderness of the block.

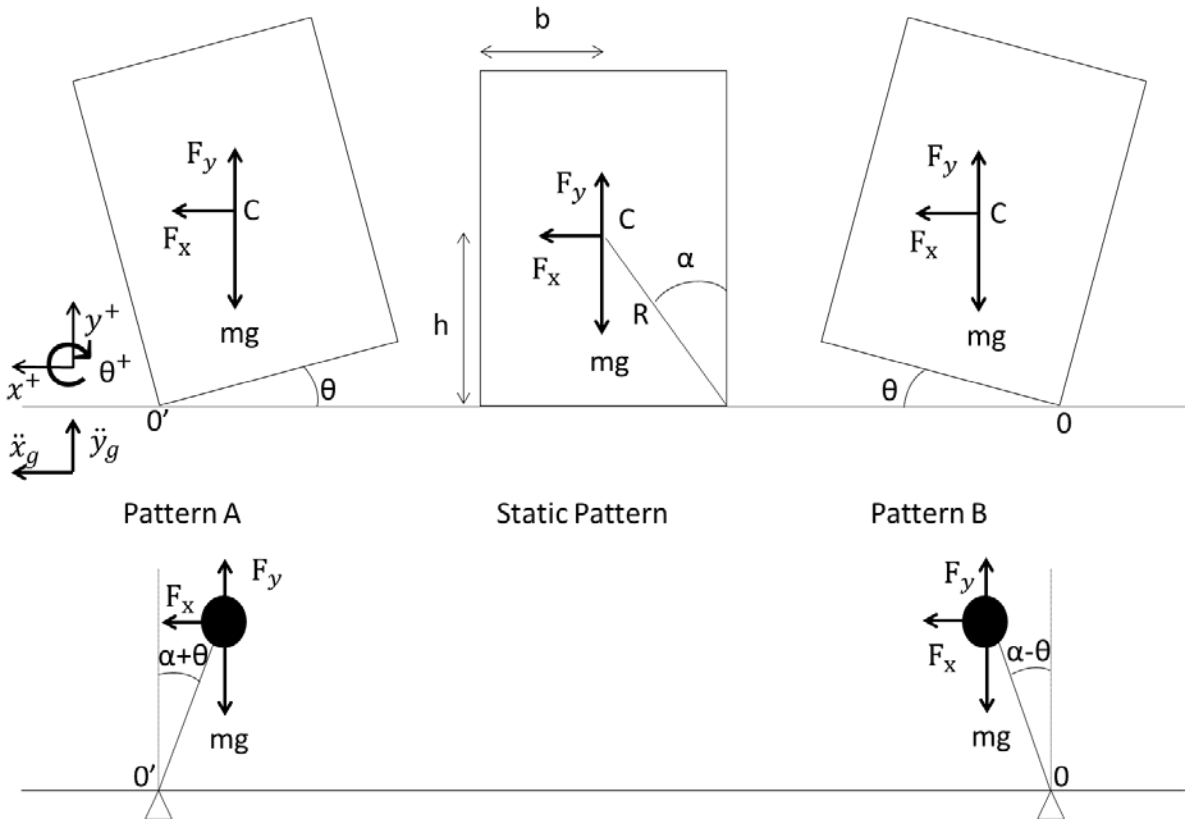


Fig. 1- Inverted Pendulum model defined by Housner [2] for a free-standing rocking block**.**

The body rocks with respect to one of the corners depending on the sign of $\theta$. Thus, it can be simulated by a pendulum whose pin is located at that corner as shown in Fig. 1. Consequently, this implies that the body cannot slide, or experience a free-flight mode, that the body and the ground are rigid, and that the response of the body is strictly planar, which are assumptions that will be followed in this paper.

The motion of the body is defined through three patterns as shown in Fig. 1: pattern A, when $\theta < 0$ , pattern B, when $\theta > 0$ and the static pattern, when $\theta = 0$ and $\dot{\theta} = 0$, i.e., when the body is at rest. The block is subjected to gravity and a horizontal, $\ddot{x}_g$ , and vertical, $\ddot{y}_g$ ,ground acceleration. $F_x$ and $F_y$ are the occuring D'Alembert forces defined by $F_x = -m\ddot{x}_g$ and $F_y = -m\ddot{y}_g$. If moments are taken about the center of rotation 0 or 0', the equations of motion, using Newton's second law, are respectively:

$$\ddot{\theta} = -p^2 \sin(\alpha - \theta) + \frac{m\ddot{x}_g}{I_0} R\cos(\alpha - \theta) - \frac{m\ddot{y}_g}{I_0} R\sin(\alpha - \theta) \text{for} \quad \theta > 0$$
$$\ddot{\theta} = p^2 \sin(\alpha + \theta) + \frac{m\ddot{x}_g}{I_0} R\cos(\alpha + \theta) + \frac{m\ddot{y}_g}{I_0} R\sin(\alpha + \theta) \text{for} \quad \theta < 0 \tag{1}$$

where $p^2 = mgh / I_0$

Fig. 2 shows the transition between patterns A and B which takes place when $\theta = 0$. During this impact, the body will experience horizontal and vertical impulses defined as $J_x$ and $J_y$ respectively.

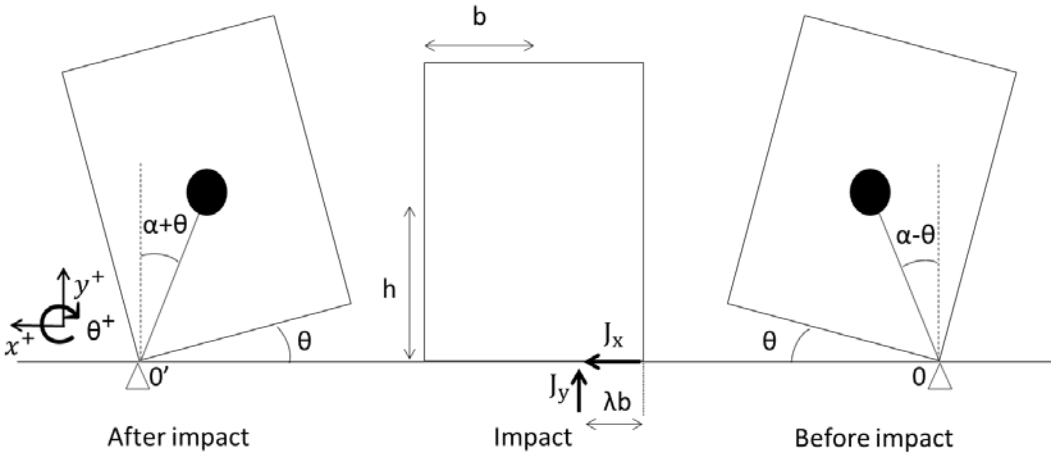


Fig. 2- A rigid body rocking from one corner to the other with impulses, $J_x$ and $J_y$ at a distance $\lambda b$.

In this study it will be assumed that the excitations are only horizontal, i.e. $\ddot{y}_g = 0$. Without any loss of generality the vertical impulse $J_y$ can be applied at a distance $\lambda b$ from the future rocking corner (assumed to be corner $0$ for the purposes of Fig. 2). In this work the often implemented in the literature assumption, that $\lambda$ is equal to zero, will be used. The angular velocity after impact is defined through the reduction of energy factor, $r$, which relates the kinetic energy before and after impact:

$$r = \frac{\left(\dot{\theta}^{+}\right)^2}{\left(\dot{\theta}^{-}\right)^2} = \frac{1/2 I_0 \dot{\theta}_2^2}{1/2 I_0 \dot{\theta}_1^2} = \left[1 - \frac{mR^2}{I_0}\left(1 - \cos\left(2\alpha\right)\right)\right]^2 \tag{2}$$

where $\dot{\theta}^{+}$ and $\dot{\theta}^{-}$ are, respectively, angular velocity after and before impact.

## 3. Earthquake Generation

In this paper, the model presented by Rezaeian and Der Kerughian in [17, 18] is used for generating the ground records. The method allows for generating ground records compatible with seismological properties such as the magnitude of the seismic event $M$, the closest distance from the recording site to the rupture area, $R_{rup}$, the shear velocity of the support ground $V_S$ and the type of the fault $F$ (corresponding to normal or strike slip). In the following a brief synopsis of the method is presented for the generation of uniaxial [17] and biaxial ground [18] motion components. Both methods are based on a list of selected earthquakes from [23] with magnitudes $M_w$ larger than 6.

### 3.1 Simulation of uniaxial ground motions.

The method develops by [17] pursues the steps shown in Fig. 3 which are explained as following:

1. Values of $M$ , $R_{rup}$ , $V_S$ and $F$ are selected as input by the user. These values are connected to a vector of auxiliary variables $v$ through stochastic equations. These equations are the result of a regression analysis from the selected database of records. Each equation has error terms which correspond to the elements of a zero mean white noise vector whose covariance matrix has been defined through the regression analysis. Having chosen the values of $M$ , $R_{rup}$ , $V_S$ and $F$ and knowing the covariance matrix of the errors, sample realizations of the $v$ vector can be obtained. This is the first level where stochasticity is introduced in the model.

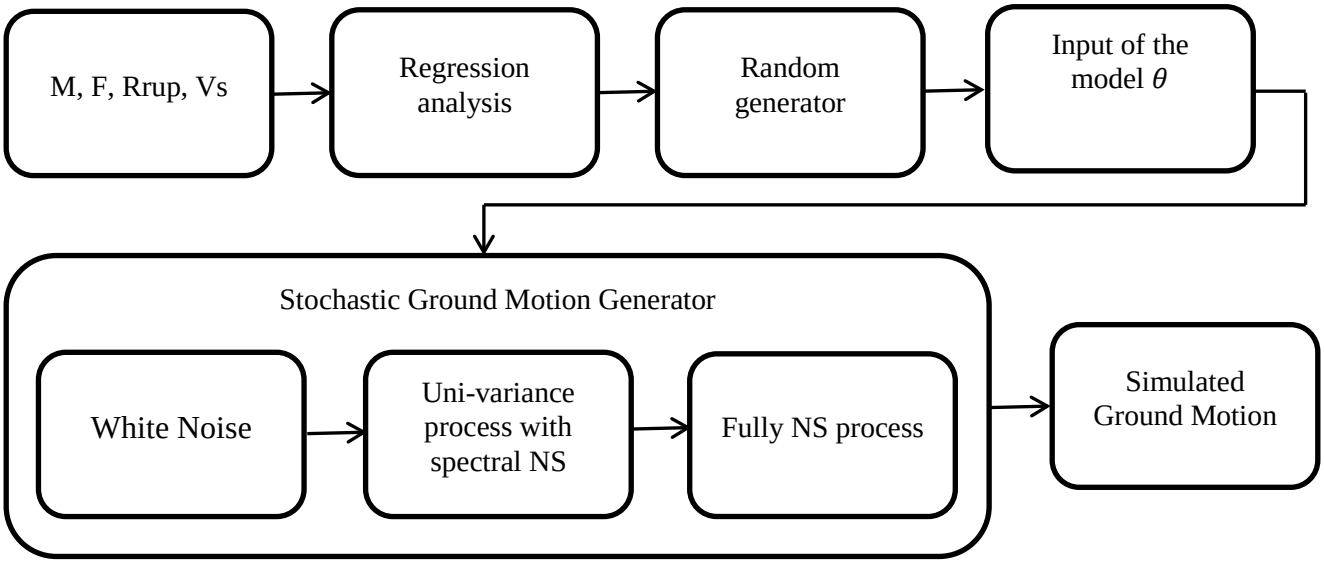


Fig. 3- Schematic explanation of the model used. NS defines the Non-Stationarity of the process.

2. Having obtained a realization of the $v$ vector the parameters of the model, $\theta$, can be obtained by using the following equations:

$$\theta_i = F_{\theta_i}^{-1}\left(\Phi\left(v_i\right)\right) \tag{3}$$

where $F_{\theta_i}$ is the cumulative distribution function (CDF) of parameter $\theta_i$ and $\Phi$ is the standard normal CDF. The probability density function (PDF) for each parameter is obtained by fitting selected PDF to the data obtained from the selected list of earthquakes. The parameters $\theta_i$ used can be separated to parameters related to the time records: the Arias Intensity $I_a$, effective duration of the record $D_{5-95}$ and time to the middle strong-shaking phase $t_{mid}$ , and model specific parameters of the stochastic model: $\omega_{mid}$ and $\omega'$ defining the frequency of the filter at any time, $t$, as $\omega_{mid} + \omega'(t - t_{mid})$ and $\zeta_f$ defining the damping of the filter.

3. The procedure for simulating the synthetic ground motion can be completed once the parameter vector $\theta$ is defined. As shown in Fig. 3, a normalized filtered white noise time-varying process is time and frequency modulated to obtain the fully Non-Stationary process $u(t)$. The time-envelope is a gamma modulating function based on the parameters $I_a$ , $D_{5-95}$ and $t_{mid}$ while the linear filter with time-varying parameters depends on $\omega_{mid}$ , $\omega'$ and $\zeta_f$ . For a given set of parameters one may obtain an arbitrary number of records through the use of a

different realization of a standard Gaussian vector. This is the second level of introducing stochasticity in the model.

### 3.2 Simulation of biaxial ground motions.

Time histories recorded at a station are a set of three records, with one of them being in the vertical direction and two in the horizontal plane. The direction at which the components are recorded in the horizontal plane does not have a specific orientation with respect to the fault. It is however of interest to determine the principal axes as described in the work of [24], i.e. the directions for which the correlation coefficients of the Arias intensity of the axes become zero [18].The occurring first principal axis is then expected to be the direction that maximizes the Arias intensity. This work further focuses on the two horizontal components, ignoring for simplicity, but without any loss of generality, the vertical component which is assumed to also be a principal component as in [18].

The method presented in [18] extends the algorithm presented in [17] discussed earlier in section 3.1, for obtaining biaxial inputs along the two principal horizontal axes, which following the convention in [18] are denoted as the major (I) and intermediate principal axes (II). As in the previous case there are six model parameters to be calibrated for each earthquake. This is achieved using the same list of selected earthquakes as in [17] with the exception that from each earthquake the corresponding pair of horizontal axes is rotated to obtain the time histories along the principal horizontal axes, before following the regression analysis for calibrating the stochastic equations that connect the seismic quantities $M$ , $R_{rup}$ , $V_S$ and $F$ to the parameters of the model.

Once the input of the model, $\theta$ is calculated as in eq. (3), the stochastic process as defined in Fig. 3 takes place. As a result, the method generates synthetic pairs of horizontal ground motion components along the principal axes.

### 3.3 Planar response of Rocking Body

The time histories generated using the methods described in sections 3.1 and 3.2 can be associated using the following Figure:

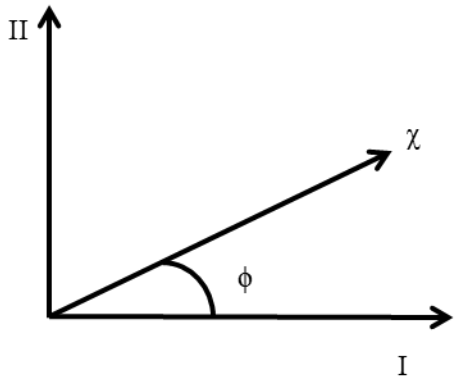


Fig. 4 - Principal axes. I and II correspond to the major and intermediate axes, respectively. $\phi$ is the angle with $\chi$

The method of section 3.2 generates a pair of time histories along the principal directions I and II, while the method of section 3.1 generates a single time history along an axis $\chi$ which generally forms some random angle $\phi$ with axis I. It is further worth mentioning that this angle $\phi$ is different for each of the uniaxial time histories generated by the method of section 3.1.

As discussed in [6] the response of rocking bodies is a generally 3D rocking response even for uniaxial horizontal inputs, unless the body is symmetric and the axis of excitation happens to be parallel with one of the axes of symmetry of the body. This work further demonstrated that the case of planar rocking is not the most conservative scenario for the body. An exception to this is when the third dimension of the body, considered to be a rectangular prism, its length $w$ , defined in Fig. 5a,is substantially bigger than the width $b$ and comparable or bigger to the height $h$ . In that case, planar rocking becomes a conservative assumption as practically only the

component of excitation parallel to the weak axis, $x$, of the body induces rocking. If sliding is neglected, as is the assumption of the current work, then the perpendicular component, along the z axis, can be ignored.

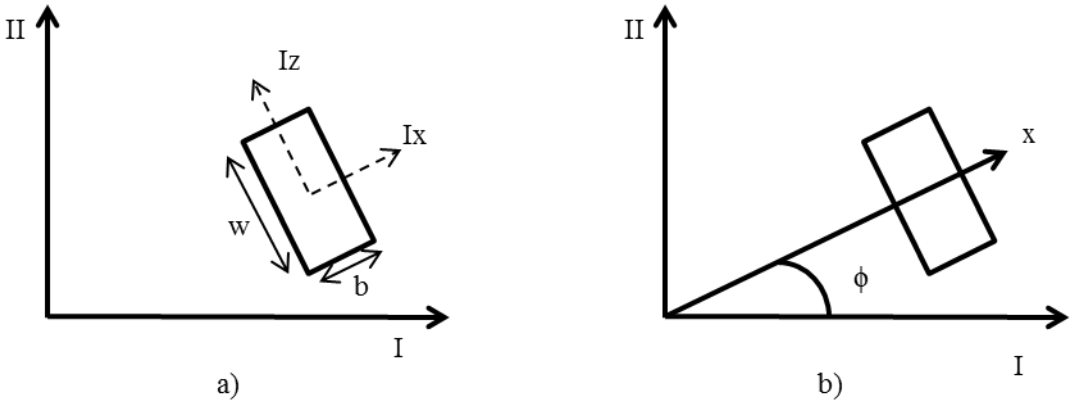


Fig. 5 a) Rectangular prims in which $w >> b$, b) rocking body twisted along the vertical axes.

In this work, the assumption that $w \gg b$ and $w \approx h$ will be used, which together with the rest of the assumptions attributed to the IPM allow for examining planar rocking as a conservative scenario. When the method of section 3.1 is used to generate the uniaxial horizontal inputs, this input is assumed to be parallel to the weak axis of the body, x. In this case, and under the previously defined assumptions, the input to the IPM is simply $\ddot{x}_g = a_\chi$.

When the method of section 3.2 is used to generate the biaxial inputs along the horizontal principal axes it will be assumed that the rocking body is twisted along the vertical axis so that its weak axis, x, forms an angle $\phi$ with axis I as shown in Fig. 5b. The input to the IPM in that case is:

$$\ddot{x}_g = a_I \cos\phi + a_{II} \sin\phi \tag{4}$$

while the perpendicular horizontal component parallel to the strong axis, z, is ignored.

## 4. Results

The rigid body selected for this study has the following dimensions: $h = 1.5565$ and $b = 0.3975$. Artificial earthquakes are generated using the methods described in section 3.The earthquakes are generated for magnitudes $M_w$ between 6 and 8.5, for a reverse fault, assuming shear velocity for the soil of $V_S = 600 m/s$ and fault rupture distance $R_{rup} = 10 Km$.

The probability of failure of the body is calculated using as intensity measure the magnitude of the earthquakes $M_w$. For that end, for each value of $M_w$ a number of artificial earthquakes were generated and introduced as inputs to the model as described in section 3.3.

### 4.1 Probability of failure curves for the generated uniaxial ground motions.

In Fig. 6a, the probability of failure of the body for different values of $M_w$, for a different number of earthquakes is presented. It should be noted that as the number of earthquakes used for each magnitude is increased the curves become more similar and convergence of the estimated probability is achieved within a margin of error. For the case examined here, it should be noted that the generation of approximately 6000 earthquakes per magnitude are required in order to estimate all probabilities with an accuracy of 2%.

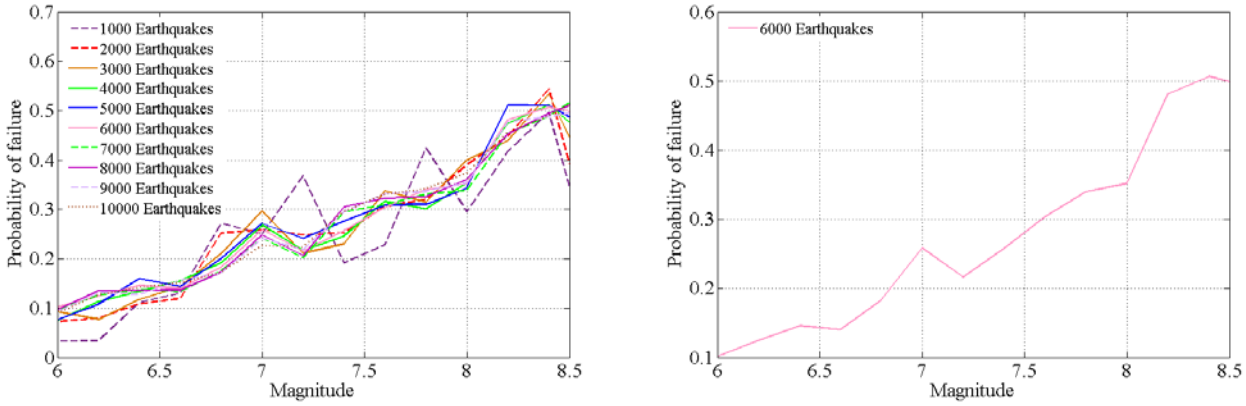


a) b)

Fig. 6 - Probability of failure curves using the uniaxial method, a) for different number of earthquakes and b) the probability of failure when the method convergences.

Having performed a convergence analysis, Fig. 6b can be used to further discuss properties of the curve. As can be observed the larger probabilities of failure of the body are observed in the region of the larger values of $M_w$. However, due to the non-lineartity of the problem, a monotonic increase of the probability of failure is not observed. In fact, there are cases where the curve locally decreases as $M_w$ increases as for example in the interval $M_w$ $[7, 7.5]$

## 4.2 Probability of failure curves for the generated biaxial ground motions.

As is mentioned in section 3.2, the biaxial inputs are generated along both horizontal principal axes, while it is assumed that the rocking body is twisted so that its local $x$ axis forms an angle $\phi$ with axis I. Due to the double symmetry of the body only values of $\phi$ in the interval $[0, 90]$ are examined in Fig. 7.

Fig. 7 shows the probability of failure curves for different values of the initial twist $\phi$. As $\phi$ is increased, it can be seen that practically the probability of failure decreases for any value of $M_w$. This is, of course, expected as the assumption that $\phi = 0^\circ$ corresponds to the scenario where the weak axis of the body, $x$, is always aligned with the major principal axis of the earthquake, while the case of $\phi = 90^\circ$ where corresponds to the strong axis of the body, $z$, being aligned with the major principal axis. Both scenarios are of course not very likely to happen in practice and hence the corresponding probabilities of failure should be seen as the upper and lower bounds of the expected probability of failure.

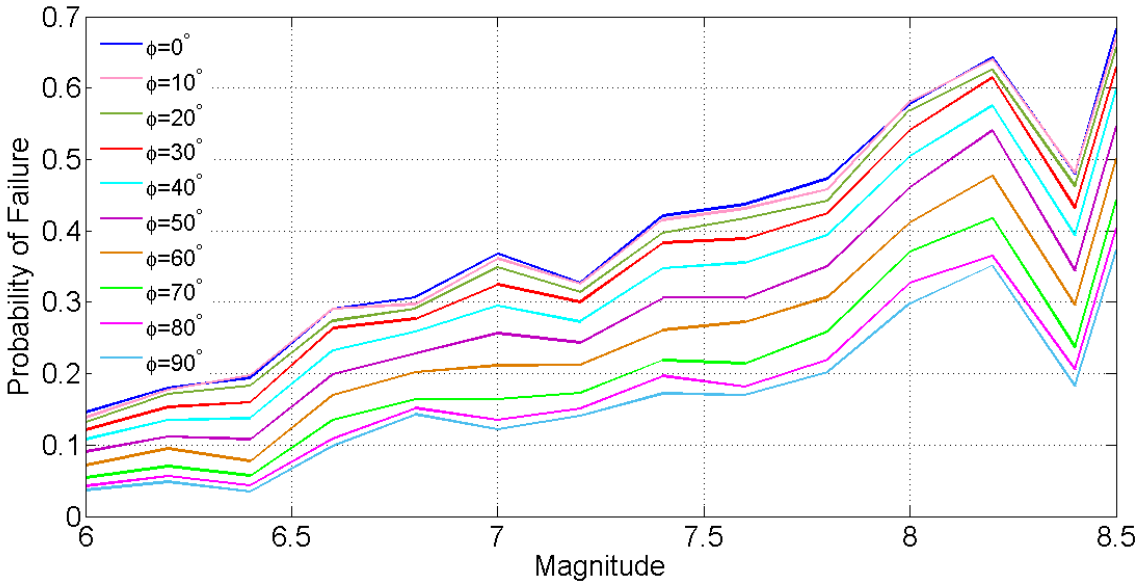


Fig. 7 – Probability of failure curves generated using the biaxial method for different values of $\phi$

In reality, the initial twist of the body $\phi$ is a random variable. We can further assume that this is a uniformly distributed random variable between $0^o$ and $360^o$. The probability of failure of the body for a magnitude $M_w$ follows eq. (5).

$$P_{M_w} = \int_{x=0^\circ}^{90^\circ} P_{M_w|\phi=x} pdf\left(x\right) dx \tag{5}$$

where, making use of the double symmetry of the body, its probability density function is: $pdf\left(x\right) = 1/90^o$. The integral of eq. (5) is computed numerically using a trapezoid integration rule. As in the case of uniaxial inputs, the probability curves are plotted for varying the number of pairs of earthquakes used and the results are presented in Fig. 8. Convergence is achieved using 4000 pair of earthquakes along the principal directions for each value of $M_w$. At this point, it should be reminded that the probability calculated from eq. (5) and shown in Fig. 8 is directly comparable to the probabilities obtained from the uniaxial inputs which are shown in Fig. 6. In both cases, the probability of failure for the body is obtained for different values of $M_w$ taking into account the randomness of the twist of the body with respect to the principal axes. However, in the case of the uniaxial inputs, each new generated sample accounts for both the randomness underlying ground motion stochastic process and the twist of the body. On the other hand for the case of the biaxial inputs used in section 4.2 these two sources of randomness are treated independently: no new ground motions need to be generated for different values of $\phi$.

As can be seen in Table 1 shows the maximum error of the probability of failure for different number of $\phi$ angles taken into account for eq. (5). Error1 is calculated for $\phi = 0, 5, 10, ...90^\circ$ and Error2 for $\phi = 0, 10, 20...90^\circ$ as the maximum difference of the probabilities calculated by varying the numbers of pairs used. Retaining the same number of generated pairs of earthquakes, the maximum error of the probability of failure decreases as more angles are taken into account. This hence allows for reducing the number of ground motions generated to achieve a desired level of convergence, by increasing the number of the values of $\phi$ used instead. The focus of the latter strategy is not to reduce the overall computational cost, although there are methods that might result into computational benefits from separating the two sources of uncertainty, but rather to reduce the required

number for the generated ground motions. The latter is desirable, as there the generation of several pair of earthquakes from a small number of experimental data results into theoretical problems [16].

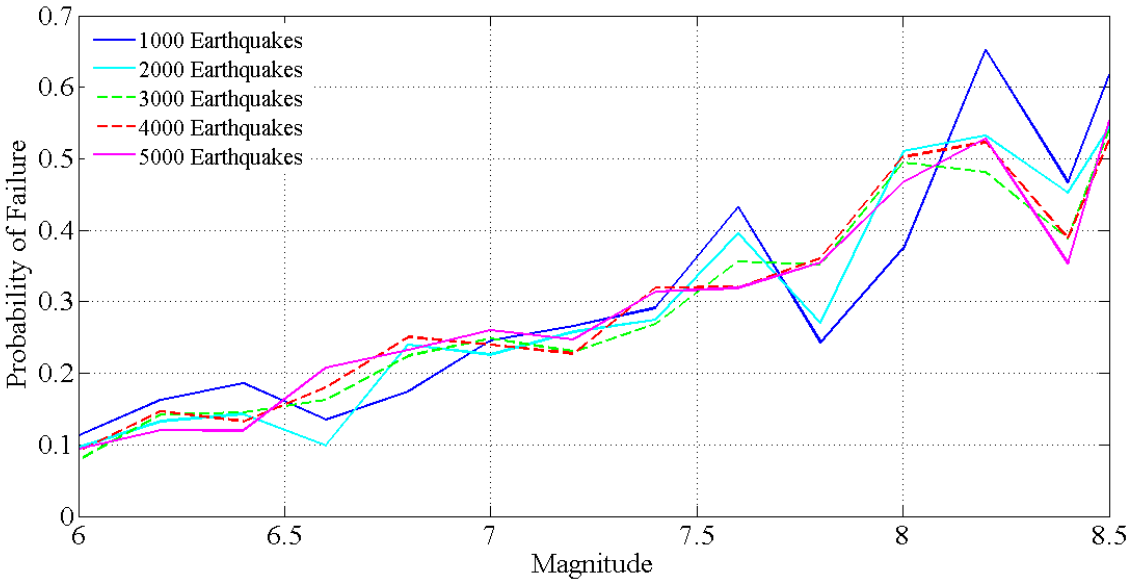


Fig. 8 - Probability of failure generated using the biaxial method for different number of earthquakes. .

Table 1 - Error Biaxial Method

| Number of earthquakes used | 1000 - 2000 | 2000 - 3000 | 3000 - 4000 | 4000 - 5000 |
|---|---|---|---|---|
| Error1 ($\phi$=0, 5, ….,90) | 6.82 | 4.11 | 2.52 | 1.26 |
| Error2 ($\phi$=0, 10, ….,90) | 7.14 | 4.23 | 2.60 | 1.43 |

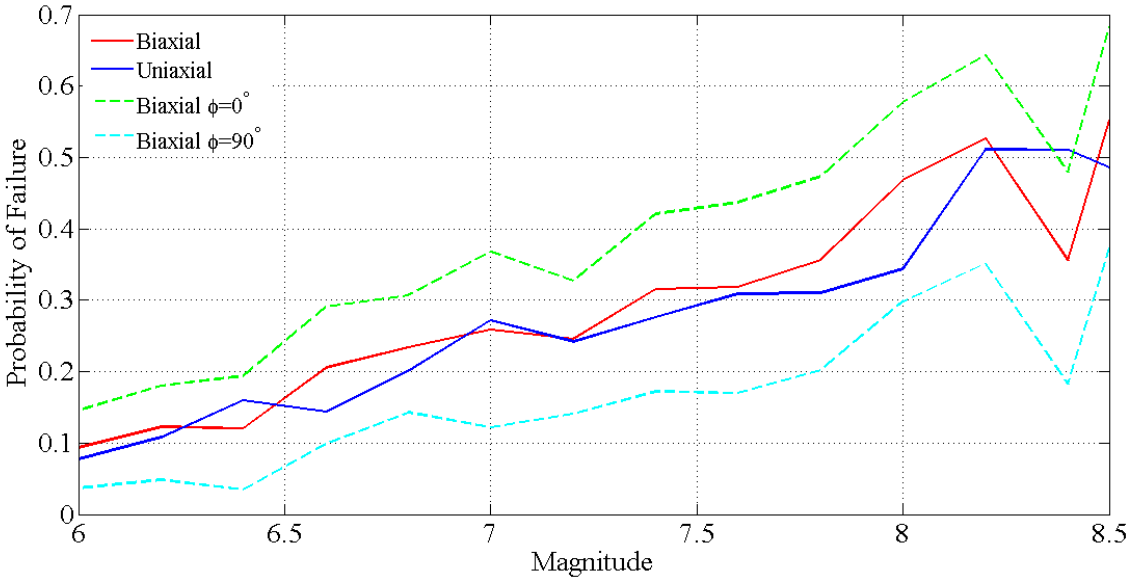


Fig. 9 – Comparison between the convergence of uniaxial and biaxal method with the biaxial method for angles $\phi = 0^o$ and $90^o$.

Finally, a comparison of the uniaxial and biaxial methods is presented in Fig. 9, where it can be seen that the probability of failure from the uniaxial method and the biaxial methods are both enveloped from the estimates of the biaxial method for angles $\phi = 0^o$ and $90^o$. An exception occurs near the maximum $M_w$ of 8.5, which is to a point expected as the list of earthquakes used to calibrate both models of section 3 contains very few earthquakes with $M_w > 8$ and hence the results obtained in that region should be addressed with some skepticism.

## 5. Conclusions

In this work the probability of failure for rocking bodies is calculated for varying the magnitude of the seismic event. To achieve so the two methods proposed in the works of [17, 18], which generate uniaxial records along a random direction and biaxial records along the principal axes, are used. It is further assumed that the length of the body is substantially bigger than the width and comparable to the height, so that the response of the body can reasonably be approximated as planar, as discussed in 12[6]. By further assuming that sliding and free flight can be neglected, this preliminary study uses the IPM as the deterministic model.

In terms of rocking, the uniaxial method of section 3.1 generates ground records that are not in general parallel to any of the principal axes. Taking into account the random twist of the rocking body with respect to the axes it can be assumed that the weak (planar rocking) axis of the body is aligned with this direction. In that sense, the method attempts to depict both the underlying stochastic nature of the earthquakes and the uncertainty of the initial twist of the body by generating more samples. It is then seen that in order for the method to converge within a desired margin of tolerance several time histories are required to be generated. It was also further shown that, similarly to what has been noticed for cycloidal pulses [9, 10] the probability of failure does not monotonically increasing as the intensity measure increases.

In contrast, the biaxial method presented in section 3.2 generates a pair of records along the principal axes. The uncertainty about the twist of the body with respect to those axes is treated independently by introducing the uniformly distributed twist $\phi$. This approach allows for providing limit estimates of the probability of failure by using the extreme values of $\phi = 0^o$ and $90^o$. The separation of the sources of uncertainty however, further allows for achieving convergence of the probability of failure within a window of tolerance by using more values of $\phi$ while retaining or even reducing the number of pairs of earthquakes generated.

Overall this paper, illustrates the use of methods for calculating the probability of failure of rocking bodies using the magnitude of earthquake as an intensity measure and further highlights the already recognized importance of making use of the notion of principal axes [24]. The latter becomes a necessity in the general case where a rocking body may experience three-dimensional rocking.

## 6. Acknowledgements

The authors would like to acknowledge the financial support of the EC, FP7-PEOPLE-2013, Marie Curie, Career Integration Grant, ‘RERCSGM’, project number 618359.

## 7. References

[1] R. L. Nigbor, S. Masri, M. Agbabian (1994): *Seismic vulnerability of small rigid objects. Proceedings of the 5th U.S. natural Conference of Earthquake Engineering*, 725-734.

[2] G. W. Housner (1963): The behaviour of inverted pendulum structures during earthquakes. *Bulleting of the Seismological Society of America*, 53, 403-417.

[3] H. Shenton , N. P. Jones (1991): Base Excitation of Rigid Bodies. I: Formulation. *Journal of Engineering Mechanics*, **117** (10).

[4] Y Ishiyama (1982): Motion of Rigid bodies and criteria for overturning by earthquake excitation. *Earthquake Engineering & Structural Dynamics*, **10** (5), 635-650.

[5] M. N. Chatzis, A. W. Smyth (2012): Robust modeling of the rocking problem. *Journal of Engineering Mechanics*, 3, 247-262.

[6] M. N. Chatzis, A. W. Smyth (2012): Modeling of the 3D rocking problem. *International Journal of Non-linear Mechanics*, 47, 85-98.

[7] A. Contento, D. Zulli, A. Egidio (2013): Seismic Behavior of monolithic objects: A 3D approach. *Engineering Seismology, Geotechnical and Structural earthquake Engineering*, 4.

[8] H. Zhang, B. Brogliato, C. Liu (2012): Study of the Planar Rocking-Block Dynamics with Coulomb Friction: Critical Kinetic Angles. *Journal of Computational non-Linear Dynamics*, **8** (2).

[9] J. Zhang, N. Makris (2001): Rocking response of free-standing blocks under cycloidal pulses. *Journal of Engineering Mechanics*, **127** (5), 473-483.

[10] R. Plaut, L. Virgin (1996): Fractal behavior of an asymmetric rigid block overturning due to harmonic motion of a tilded foundation. *Chaos, Solitons and Fractals*, **7** (2), 177-196.

[11] J. Baker (2011): Conditional Mean Spectrum: Tool for ground motion selection. *Journal of Engineering Mechanics*, 137, 322-331.

[12] M. Shinozuca, G. Deodatis (1991): Simulation of stochastic processes by spectral representation. *American Society of Mechanical Engineering*, **44** (4), 191-204.

[13] P. Cacciola, G. Deodatis (2011): A method for generating fully non-stationary and spectrum-compatible ground motion vector processes. *Soil Dynamics and Earthquake Engineering*, **31** (3), 351-360.

[14] M. D. Purvance, A. Anooshehpoor, J. N. Brune (2008): Freestanding block and overturning fragilities: Numerical simulation and experimental validation. *Earthquake Engineering & Structural Dynamics*, 37, 791-808.

[15] G. P. Mavroeidis, A. S. Papageorgiou (2003): A mathematical representation of near fault ground motions. *Bulleting of the Seismological Society of America*, **93** (3), 1099-1131.

[16] A. Olivier, A. W. Smyth: Tradeoffs between statistical agreement and data reproduction in the generation of synthetic ground motions. *Probabilistic Engineering Mechanics.*

[17] S. Rezaeian, A. Der Kiureghian (2010): Simulation of synthetic ground motions for specified earthquake and site characteristics. *Earthquake Engineering & Structural Dynamics*, **39** (10), 1155-1180.

[18] S. Rezaeian, A. Der Kiureghian (2012): Simulation of orthogonal horizontal ground motion components for specified earthquake and site characteristics. *Earthquake Engineering & Structural Dynamics*, **41** (2), 335-353.

[19] R. W. Clough, J. Penzien (1975). *Dynamics of Structures*. Mcgraw-Hill.

[20] C. S. Yim, A.K. Chopra, J. Penzien (1980): Rocking response of rigid bodies to earthquakes. *Earthquake Engineering & Structural Dynamics*, **8** (6), 565-587.

[21] E. G. Dimitrakopoulos, T. S. Paraskeva (2015): Dimensionless fragility curves for rocking response to near-fault excitations. *Earthquake Engineering & Structural Dynamics*, **44** (12), 2015-2033.

[22] S. Acikgoz, m. J. DeJong (2014): The rocking response of large flexible structures to earthquakes. *Bulletin of Earthquake Engineering*, 12, 875-908.

[23] W, Campbel, Y. Bozorgnia (2008): NGA ground motion model for the geometric mean horizontal component of PGA, PGV, PGD and 5% damped linear elastic response spectra for periods ranging from 0.01 to 10s. *Earthquake Spectra*, 24, 139-171.

[24] J. Penzien, M. Watabe (1975): Characteristics of 3-dimensional earthquake ground motions. *Earthquake Engineering & Structural Dynamics*, 13, 1-12.